AGU PUBLICATIONS

JGR

Journal of Geophysical Research: Space Physics

RESEARCH ARTICLE

10.1002/2014JA020443

Key Points:
- Approximate analytical solutions for trapped electron distributions
- Reproduces simulations during quiet and storm times
- Could allow to infer average wave characteristics from measured distributions

Correspondence to:
D. Mourenas,
didier.mourenas@gmail.com

Citation:
Mourenas, D., A. V. Artemyev, O. V. Agapitov, V. Krasnoselskikh, and W. Li (2014), Approximate analytical solutions for the trapped electron distribution due to quasi-linear diffusion by whistler mode waves, *J. Geophys. Res. Space Physics*, *119*, 9962–9977, doi:10.1002/2014JA020443.

Received 28 JUL 2014
Accepted 22 NOV 2014
Accepted article online 27 NOV 2014
Published online 18 DEC 2014

Approximate analytical solutions for the trapped electron distribution due to quasi-linear diffusion by whistler mode waves

D. Mourenas[1], A. V. Artemyev[1,2], O. V. Agapitov[3,4], V. Krasnoselskikh[1], and W. Li[5]

[1]LPC2E/CNRS-University of Orleans, Orleans, France, [2]Space Research Institute, RAS, Moscow, Russia, [3]Space Science Laboratory, University of California, Berkeley, California, USA, [4]National Taras Shevchenko University of Kiev, Kiev, Ukraine, [5]Department of Atmospheric and Oceanic Sciences, University of California, Los Angeles, California, USA

Abstract The distribution of trapped energetic electrons inside the Earth's radiation belts is the focus of intense studies aiming at better describing the evolution of the space environment in the presence of various disturbances induced by the solar wind or by an enhanced lightning activity. Such studies are usually performed by means of comparisons with full numerical simulations solving the Fokker-Planck quasi-linear diffusion equation for the particle distribution function. Here we present for the first time approximate but realistic analytical solutions for the electron distribution, which are shown to be in good agreement with exact numerical solutions in situations where resonant scattering of energetic electrons by whistler mode hiss, lightning-generated or chorus waves, is the dominant process. Quiet time distributions are well recovered, as well as the evolution of energized relativistic electron distributions during disturbed geomagnetic conditions. It is further shown that careful comparisons between the analytical solutions and measured distributions may allow to infer important bounce- and drift-averaged wave characteristics (such as wave amplitude). It could also help to improve the global understanding of underlying physical phenomena.

1. Introduction

Satellites crossing repeatedly the Earth's inner or outer radiation belts incur a risk of being damaged or even lost by their prolonged exposure to the intense energetic electron fluxes which populate these regions of the magnetosphere [*Horne et al.*, 2013]. Such electron fluxes can vary dramatically during strong magnetic storms or other disturbances driven by the solar wind [e.g., see *Shprits et al.*, 2006, 2008; *Turner et al.*, 2013; *Thorne et al.*, 2013, and references therein]. Inside the radiation belts (at $L < 6$), these variations are due to a combination of (and competition between) radial diffusion, losses due to pitch angle scattering by whistler mode waves (or ion cyclotron waves), and acceleration via energy diffusion by the same waves [*Kennel and Petschek*, 1966; *Trakhtengerts*, 1966; *Lyons et al.*, 1972; *Lyons*, 1974; *Summers et al.*, 1998; *Brautigam and Albert*, 2000; *Meredith et al.*, 2009; *Shprits et al.*, 2008; *Thorne*, 2010].

To be able to understand and forecast the Earth's radiation belts evolution, it is therefore essential to better assess the relative importance of these various processes. One way of doing this is to establish average models of the different wave distributions based on satellite statistics [*Horne et al.*, 2005; *Agapitov et al.*, 2013; *Bunch et al.*, 2013; *Li et al.*, 2013a; *Mourenas et al.*, 2014]. Another way is to examine the measured in situ electron distributions during given periods of time, to try to infer both the wave characteristics and distribution during such events, and also to check which process was actually dominant at that time [e.g., see *Li et al.*, 2013b; *Thorne et al.*, 2013; *Ni et al.*, 2014].

The detailed electron differential fluxes measured by the CRRES and SAMPEX satellites as a function of time and L have allowed for significant advances in our understanding of the radiation belts [e.g., see *Baker et al.*, 1994; *Brautigam and Albert*, 2000; *Horne et al.*, 2005; *Meredith et al.*, 2009; *Su et al.*, 2011]. Now even more precise and detailed information are becoming available from the recent Van Allen Probes [e.g., *Thorne et al.*, 2013; *Baker et al.*, 2014; *O'Brien et al.*, 2014]. However, to gain new insights, satellite measurements have to be compared with large-scale numerical simulations [*Shprits et al.*, 2006; *Thorne et al.*, 2013; *Li et al.*, 2014a] solving the Fokker-Planck equation describing the evolution of the trapped energetic electron distribution due to quasi-linear scattering by whistler mode waves of limited amplitude (typically $<$ 300 pT

for > 1 MeV electrons at $L \leq 6$ for quasi-linear diffusion to prevail over nonlinear effects) [see *Tao et al.*, 2012]. While *Schulz and Lanzerotti* [1974] have already derived interesting analytical solutions (eigenmodes) for the particle distributions, they used arbitrarily prescribed (nonrealistic) formulations of the diffusion rates.

Here we derive for the first time *realistic analytical expressions* for the electron distribution, obtained by solving the corresponding diffusion equations, making use of previously obtained approximate analytical formulations of the pitch angle and energy diffusion coefficients, as well as of the characteristic lifetimes of electrons in the case of quasi-parallel (or oblique) whistler mode waves [*Mourenas and Ripoll*, 2012; *Mourenas et al.*, 2012b; *Artemyev et al.*, 2013b; *Mourenas et al.*, 2014]. The derived analytical electron distributions are compared with full numerical solutions, demonstrating a good agreement during quiet as well as disturbed geomagnetic conditions, for hiss and lightning-generated waves at $L \leq 3$ and chorus waves at $L \sim 5$.

Finally, we show that the obtained analytical expressions could be useful to infer some characteristics of the dominant waves during selected events. In particular, we recover the average measured wave amplitude by means of careful comparisons between measured electron distributions at different energies and times with the analytical solutions. The latter should also help to better understand the occurring processes by allowing quick and easy comparisons of observed distributions with the general behavior of the analytical expressions.

2. Analytical Expressions of the Trapped Electron Distribution

2.1. Generalities

Following previous works [e.g., see *Lyons et al.*, 1972; *Albert*, 1994; *Albert and Shprits*, 2009], we first assume here that the electron distribution function f satisfies a one-dimensional Fokker-Planck pitch angle diffusion equation in a dipolar geomagnetic field

$$\frac{\partial f}{\partial t} = \frac{1}{T_b \sin 2\alpha_0} \frac{\partial}{\partial \alpha_0} (\langle D_{\alpha\alpha} \rangle T_b \sin 2\alpha_0 \frac{\partial f}{\partial \alpha_0}) \tag{1}$$

where $\langle D_{\alpha\alpha} \rangle (\alpha_0)$ is the bounce-averaged pitch angle diffusion coefficient (in s^{-1}) and T_b is the bounce period of electron oscillations between their mirror points. In this case, the electron distribution function evolves mainly due to quasi-linear pitch angle scattering by whistler mode waves (with related losses into the atmospheric loss cone). Further, assuming that the late-time asymptotic full distribution can be written as a product of time-dependent and time-independent functions as $f(\alpha_0, t) \sim g(\alpha_0) F(t)$ with an exponentially decaying $F(t) = \exp(-t/\tau_L)$, one gets

$$\frac{\partial}{\partial \alpha_0} (\langle D_{\alpha\alpha} \rangle T_b \sin 2\alpha_0 \frac{\partial g}{\partial \alpha_0}) + \frac{T_b \sin 2\alpha_0 g}{\tau_L} = 0 \tag{2}$$

where τ_L is the characteristic lifetime of the considered electrons in the radiation belt [*Schulz and Lanzerotti*, 1974; *Albert and Shprits*, 2009].

2.2. Case 1: Quasi-Parallel Waves and High-Energy Electrons at Not-Too-Low *L*

First, we consider *quasi-parallel* whistler mode waves (such as high-amplitude chorus in the outer belt, or hiss, lightning-generated, or VLF waves inside the plasmasphere at $L > 1.5$). Previously derived approximate analytical expressions of $\langle D_{\alpha\alpha} \rangle$ and τ_L for first-order cyclotron resonance can be used to simplify equation (2).

Namely, it was found in previous works that $\tau_L = \eta/(2\langle D_{\alpha\alpha}(\alpha_{LC}) \rangle)$ (where α_{LC} denotes the loss cone angle) with $\eta \sim 1$, while $\langle D_{\alpha\alpha}(\alpha_0) \rangle \sim \langle D_{\alpha\alpha}(\alpha_{LC}) \rangle / \cos^2(\alpha_0)$ from α_{LC} up to $\alpha_{0,M} \sim \min(\pi/2 - \theta_{max}, \alpha_{0,i})$ where $\cos \alpha_{0,i} = 1/(p\epsilon_{UC})$ [*Mourenas et al.*, 2012b; *Artemyev et al.*, 2013b]. Here $\theta_{max} < 45°$ is the upper bound on the wave normal angle distribution of quasi-parallel waves, $\epsilon_{UC} = \sqrt{\omega_{UC}/\Omega_{ce0}} \Omega_{pe0}/\Omega_{ce0}$ where ω_{UC} is the upper limit of the wave frequency distribution and Ω_{pe0} and Ω_{ce0} are the equatorial electron plasma frequency and gyrofrequency, respectively (p being the electron momentum normalized to $m_e c$).

It is further assumed at this stage that $\tan \alpha_0 \langle D_{\alpha\alpha} \rangle \geq \tan \alpha_{LC} \langle D_{\alpha\alpha}(\alpha_{LC}) \rangle$ for $\alpha_0 \geq \alpha_{0,M}$, in which case the lifetime of electrons is mainly determined by the low pitch angle part of the diffusion rate [e.g., see *Albert and Shprits*, 2009; *Artemyev et al.*, 2013b]. When only whistler mode waves are present, this corresponds to typical profiles of $\langle D_{\alpha\alpha}(\alpha_0) \rangle$ for high-enough electron energy and/or $\Omega_{pe0}/\Omega_{ce0}$ and/or ω_{UC}/Ω_{ce0} such that $p\epsilon_{UC} \geq 10$. Nonetheless, when additional wave populations coexist with the considered low-to-medium

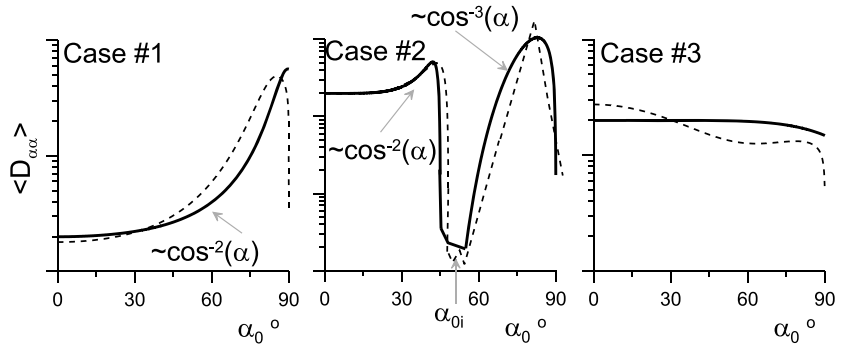

Figure 1. Typical profiles of $\langle D_{\alpha\alpha} \rangle$ as a function of α_0 corresponding to Cases 1, 2, and 3. The typical shapes assumed here are shown by solid lines, while examples of other shapes expected to yield similar lifetimes and electron distributions are displayed with dashed lines. (left) Case 1 corresponds to high-energy electrons interacting with low-frequency quasi-parallel whistler mode hiss and lightning-generated waves at $L \sim 3$–5 [e.g., see right panel in middle row of Figure 4 in the work by *Meredith et al.*, 2009] or medium- to high-energy electrons interacting with quasi-parallel chorus waves during periods of high geomagnetic activity at $L > 4$ (e.g., see Figure 3 in the work by *Mourenas et al.* [2014]). (middle) Case 2 corresponds to not-too-high energy electrons interacting with low-frequency hiss parallel waves at $L \leq 3$ (e.g., see left panel in middle row of Figure 4 in the work by *Meredith et al.* [2009]). (right) Case 3 corresponds to the presence of VLF (e.g., from terrestrial transmitters) waves becoming very oblique at high latitudes [see *Agapitov et al.*, 2014; *Mourenas et al.*, 2014].

frequency whistlers, such as higher-frequency whistlers (e.g., upper band chorus or VLF waves) [see *Meredith et al.*, 2012; *Agapitov et al.*, 2014] or very oblique fast magnetosonic waves [*Mourenas et al.*, 2013], the trough in scattering rate at large α_0 can be filled enough to relax the above condition $p\epsilon_{UC} \geq 10$ [*Artemyev et al.*, 2013b; *Mourenas et al.*, 2013]. The typical profiles of $\langle D_{\alpha\alpha} \rangle$ corresponding to Case 1 are displayed in Figure 1.

Moreover, T_b is known to vary weakly with α_0. Accordingly, taking $T_b \approx cte$ in equation (2) and replacing $\langle D_{\alpha\alpha} \rangle$ and τ_L by their approximate analytical expressions (see Appendix A), one finally gets a simple second-order differential equation for the asymptotic (in time) steady shape of g

$$\frac{\partial^2 g}{\partial \alpha_0^2} \tan \alpha_0 + \frac{\partial g}{\partial \alpha_0} \sec^2 \alpha_0 + g \frac{\sin 2\alpha_0}{\eta} = 0 \tag{3}$$

The general analytical solution of the above equation can be expressed as a linear combination of modified Bessel functions of the first kind (I_0) and second kind (K_0) [*Abramowitz and Stegun*, 1972] with real or complex multipliers. Since we are looking here for a real-valued g, it is worth noting that $\Im(K_0(y)) + i\pi I_0(y)/2 = 0$. As a result, g can be more simply cast as a sum of I_0 and $\Re(K_0)$ functions as

$$g(\alpha_0) = c_1 I_0(i\sqrt{2/\eta} \sin \alpha_0) + c_2 \Re(K_0(i\sqrt{2/\eta} \sin \alpha_0)) \tag{4}$$

where c_1 and c_2 are real numerical coefficients and $i = \sqrt{-1}$.

We shall now proceed to demonstrate that existing additional constraints on the electron distribution will fully determine the unknown coefficients c_1 and c_2. The function g must indeed be null at the loss cone edge $g(\alpha_{LC}) = 0$, while the relation $\partial g/\partial \alpha_0 = 0$ must be satisfied at $\alpha_0 = \pi/2$ [*Lyons et al.*, 1972; *Albert*, 1994]. The latter condition is actually always fulfilled by the analytical solution (4) because of the intrinsic property $\partial I_0(i\sqrt{2} \sin \alpha_0)/\partial \alpha_0 = \partial K_0(i\sqrt{2} \sin \alpha_0)/\partial \alpha_0 = 0$ for $\alpha_0 = \pi/2$. Finally, a proper normalization of g requires that $2\int_{\alpha_{LC}}^{\pi/2} g \sin \alpha_0 d\alpha_0 = 1$. Thus, there are two conditions for two unknown variables, leading to one unique real solution for g.

Using condition $g(\alpha_{LC}) = 0$ in equation (4) leads straightforwardly to

$$\frac{c_1}{c_2} = \frac{-\Re(K_0(i\sqrt{2/\eta} \sin \alpha_{LC}))}{I_0(i\sqrt{2/\eta} \sin \alpha_{LC})}. \tag{5}$$

The remaining unknown variable c_2 is determined from the last condition $\int_{\alpha_{LC}}^{\pi/2} 2g \sin \alpha_0 d\alpha_0 = 1$ together with equation (5). Incidentally, it can be noted that η can be either a positive or a negative real number in the above general solution (corresponding respectively to exponential decay or growth of $F(t)$).

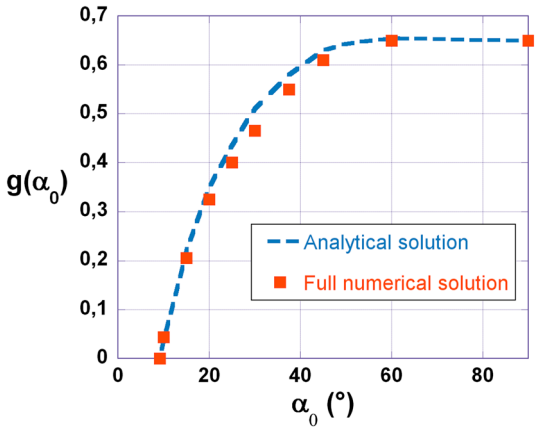

Figure 2. Profile of the asymptotic (final) electron distribution in the case of 2 MeV electrons interacting with low-frequency whistler mode waves at $L \sim 3$ during quiet conditions. The red squares show the full numerical solution of *Meredith et al.* [2009], while the blue dashed line shows the approximate analytical solution given by (4)–(6).

Typically, for quasi-parallel whistler mode waves interacting with high-energy electrons, one has $\eta \sim 1$. Then, a useful approximate formulation of (5), obtained by series of expansions and correct to within less than 8% for $1° \leq \alpha_{LC} \leq 30°$, is $c_1/c_2 \sim \ln(\sqrt{2}\sin\alpha_{LC})$. There is no simple analytical expression for c_2. Nevertheless, three approximate formulas can be obtained in the small, medium, and large α_0 limits, which should suffice for most practical purposes. One gets

$$c_2 \approx -\sin^{3/7}\alpha_{LC} \quad (\alpha_{LC} < 20°)$$
$$c_2 \approx -3\sin^{4/3}\alpha_{LC} \quad (20° \leq \alpha_{LC} \leq 40°)$$
$$c_2 \approx \frac{-4}{5\sin^3\alpha_{LC}} \quad (\alpha_{LC} > 40°) \qquad (6)$$

where the discrepancy between the above formulas and the exact solution is less than a few percents in their respective domains of validity.

To check the accuracy of our approximate analytical formulas for the electron distribution g, we have considered a test case of $E = 2$ MeV electrons interacting with hiss and lightning-generated waves at $L = 3$ provided in Figure 6 (right) in the work by *Meredith et al.* [2009]. This case satisfies all our previously stated assumptions. In Figure 2, we have plotted both our analytical formula (4) and the asymptotic (late-time) numerical solution provided by *Meredith et al.* [2009] and obtained by solving numerically the full diffusion equation. One can see that the approximate analytical solution exhibits a fairly good quantitative agreement with the full numerical solution for the trapped electron distribution, with a mean error percentage smaller than 10%.

2.3. Case 2: Low-Frequency Quasi-Parallel Waves and Relatively Low Energy Electrons at Low *L*

When the energy of the considered electrons is relatively low, or the plasma density is small, or the ratio ω_m/Ω_{ce0} is small (where ω_m is the mean frequency of the low-frequency high-amplitude waves and subscript "m" means from now on that we use $\omega = \omega_m$), so that $p\epsilon_{UC} < 10$, a deep trough in scattering rate may appear at $\alpha_0 > 35°$ such that $\tan\alpha_0\langle D_{\alpha\alpha}\rangle < \tan\alpha_{LC}\langle D_{\alpha\alpha}(\alpha_{LC})\rangle$ at least locally in the domain $\alpha_0 > \alpha_{0,M}$. Note that we shall hereafter focus on low but not too low electron energies such that $p\epsilon_{UC} < 10$ and $p\epsilon_m > 1.1$, to allow using previous analytical estimates developed in this range [*Mourenas and Ripoll*, 2012; *Mourenas et al.*, 2012b]. It corresponds roughly to $E > 400$ keV at $L \sim 2.5$–3 in the slot region for electron interaction with hiss and lightning-generated waves or $E > 100$ keV at $L \sim 4.5$–5.5 for interaction with lower band chorus waves. The typical profile of $\langle D_{\alpha\alpha}\rangle$ corresponding to Case 2 is displayed in Figure 1 (middle).

Accordingly, when a very steep (almost vertical) increase of the diffusion rate $\langle D_{\alpha\alpha}\rangle$ is encountered at $\alpha_{0,i}$ as α_0 decreases, then the situation for the high pitch angle part of the electron distribution g is roughly equivalent to the presence of a kind of loss cone at $\alpha_0 \leq \alpha_{0,i}$. Electrons scattered toward smaller α_0 should be very quickly diffused toward still smaller α_0 once they get close enough to $\alpha_{0,i}$, just like what happens near the actual loss cone. Accordingly, we conjecture that g can then be split into two separate parts $g \approx g^{<}(\alpha_0 \leq \alpha_{0,i}) + g^{>}(\alpha_0 \geq \alpha_{0,i})$, with each part having its own loss cone (or equivalent loss cone) angle at α_{LC} and $\alpha_{0,i}$, respectively.

In such a situation, the global electron lifetime will be increased as compared to Case 1, due to the much slower diffusion at high pitch angles in Case 2. Now the question that must be answered is how does it modify the shape of g? First, it can be easily shown that when the global lifetime τ_L is increased by a factor $\eta > 1$ as compared to its value for Case 1 in the high-energy range (where $\tau_L \sim 1/(2\langle D_{\alpha\alpha}(\alpha_{LC})\rangle)$), the positive slope of the analytical solution (4) for $g(\alpha_0)$ increases significantly between $\alpha_0 \sim 30°$ and $\alpha_0 \sim 90°$ when $\eta \geq 1$ increases, which actually corresponds to the observed increase of the slope of the full numerical solution of g as the global electron lifetime τ_L increases [e.g., see *Meredith et al.*, 2009].

In agreement with the shape of the most general analytical solutions (4) and (5), the two parts $g^>$ and $g^<$ of g can be roughly approximated by flat-top distributions $\langle g^> \rangle$ and $\langle g^< \rangle$ over $\alpha_0 \geq \alpha_{0,i}$ and $\alpha_{LC} < \alpha_0 < \alpha_{0,i}$, respectively. Furthermore, we make the important conjecture that upon reaching the asymptotic shape-preserving stage for the distribution g, conservation of particle flux in phase space should determine the ratio $\langle g^> \rangle / \langle g^< \rangle$ of the levels of the two parts so that it can remain constant. Specifically, the outgoing (into the loss cone) electron flux from the $\alpha_{LC} < \alpha_0 < \alpha_{0,i}$ region must be balanced by the incoming flux from the region $\alpha_0 \geq \alpha_{0,i}$. Such an equilibrium between the two (incoming and outgoing) fluxes can be written as

$$\int_{\alpha_{LC}}^{\alpha_{0,i}} \frac{\langle g^< \rangle \sin\alpha_0 d\alpha_0}{\tau_{L<}} = \int_{\alpha_{0,i}}^{\pi/2} \frac{\langle g^> \rangle \sin\alpha_0 d\alpha_0}{\tau_{L>}} \tag{7}$$

where $\tau_{L<}$ and $\tau_{L>} = \tau_{LL}$ represent the characteristic loss timescales in the two respective domains. In the high pitch angle range $\alpha_0 > \alpha_{0,i}$ corresponding to Landau resonance with quasi-parallel whistler mode waves, the scattering rate varies like $\langle D_{\alpha\alpha} \rangle \sim \cos^3\alpha_{0,i} / \cos^3\alpha_0$ [*Mourenas and Ripoll*, 2012; *Mourenas et al.*, 2012b]. Although such a variation is slightly different from the $1/\cos^2\alpha_0$ variation for cyclotron resonance in the low pitch angle range, solving numerically the corresponding second-order differential equation for $g^>$ (which does not seem to have analytical solutions) shows that $g^>(\alpha_0)$ has nevertheless a very similar shape in the vicinity of $\alpha_0 = \pi/2$. Consequently, we chose here to employ the approximation $\langle D_{\alpha\alpha} \rangle \sim \cos^2\alpha_{0,i} / \cos^2\alpha_0$ for the sake of simplicity while simultaneously using for the lifetime the appropriate analytical estimate τ_{LL} explicitly given in Appendix A [see also *Artemyev et al.*, 2013b] when the contribution from the minimum in Landau resonance scattering determines the global lifetime (i.e., when $\tau_L \sim \tau_{LL} \geq \tau_{L<}$ as assumed for Case 2). An analytical expression for $\tau_{L<}$ is also provided in Appendix A.

As a result, an approximate analytical solution for the full electron distribution g can be written under the form

$$\begin{aligned} g(\alpha_0) &= g^<(\alpha_0 < \alpha_{0,i}) + g^>(\alpha_0 \geq \alpha_{0,i}) \\ \frac{g^>}{c_3} &= \frac{\Re(K_0(iy\sin\alpha_{0,i}))I_0(iy\sin\alpha_0)}{I_0(iy\sin\alpha_{0,i})} - \Re(K_0(iy\sin\alpha_0)) \\ \frac{g^<}{c_4} &= \frac{\Re(K_0(iy\sin\alpha_{LC}))I_0(iy\sin\alpha_0)}{I_0(iy\sin\alpha_{LC})} - \Re(K_0(iy\sin\alpha_0)) \end{aligned} \tag{8}$$

with

$$\begin{aligned} y^{-2} &= \langle D_{\alpha\alpha}(\alpha_{LC}) \rangle \tau_{LL} \\ \frac{c_3}{c_4} &= \frac{(\cos\alpha_{LC} - \cos\alpha_{0,i})\tau_{LL}}{\cos\alpha_{0,i}\tau_{L<}} \\ \int_{\alpha_{LC}}^{\pi/2} 2\, g\, \sin(\alpha_0) d\alpha_0 &= 1 \end{aligned} \tag{9}$$

where c_3 and c_4 are uniquely determined by the last two equations.

We have considered in Figure 3 a test case from *Meredith et al.* [2009] in which 2 MeV electrons are scattered in pitch angle by hiss waves at $L = 2$ during quiet time. The realistic hiss spectrum with $B_w \sim 20$ pT is composed of two Gaussians such that the most intense and lowest-frequency one has $\omega_m/\Omega_{ce0} \sim 0.0032$, $\Delta\omega/\omega_m \sim 1$, $\Delta\theta = 20°$, $p\epsilon_m \sim 1.56$, while the upper frequency cutoff of the second Gaussian is fixed at 2 kHz, giving $p\epsilon_{UC} \sim 3.8$ [*Artemyev et al.*, 2013b; *Meredith et al.*, 2009]. Using the latter values, we recover approximately with analytical formulas in Appendix A the computed diffusion rates and lifetime values displayed by *Meredith et al.* [2009] in their Figure 4. Moreover, we get $c_3/c_4 \approx 185$ and $y \approx 0.3$.

The approximate analytical solution (8) is in good agreement with the full numerical solution for the trapped electron distribution over the whole pitch angle domain in Figure 3, in spite of the very large variation of g with α_0 and although our approximations do not take into account the fine details of the actual wave power spectrum. The mean relative error over $\alpha_0 = 20°$–$90°$ is about a factor of 2. In particular, the boundary $\alpha_{0,i}$ between the two regions is well recovered, as well as the ratio $\langle g^> \rangle / \langle g^< \rangle$ (within a factor of 2 for an actual increase of ~ 400), lending further credibility to the above simplified analytical solutions.

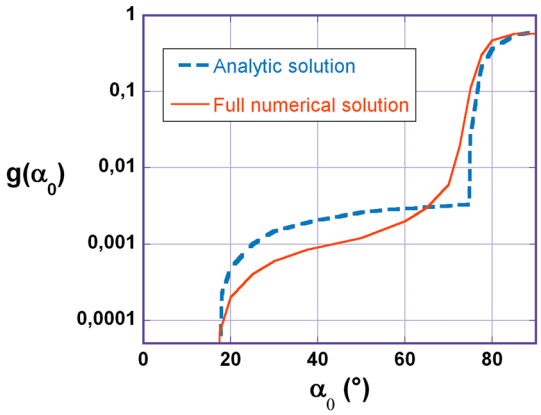

Figure 3. Profile of the (unnormalized) asymptotic (final) electron distribution in the case of 2 MeV electrons interacting with low-frequency whistler mode waves at $L \sim 2$ during quiet conditions. The red line shows the full numerical solution of *Meredith et al.* [2009], while the blue dashed line shows the approximate analytical solution given by equations (8) and (9).

2.4. Case 3: Nearly Constant $\langle D_{\alpha\alpha}(\alpha_0)\rangle$

Other analytical solutions can be derived in the case of a constant $\langle D_{\alpha\alpha}(\alpha_0)\rangle$ profile (see Figure 1 (right)). It can correspond either to a situation where oblique waves near the resonance cone are present at medium to high latitudes or when the wave power increases strongly with latitude (or both) [*Agapitov et al.*, 2013; *Artemyev et al.*, 2013a; *Mourenas et al.*, 2014; *Li et al.*, 2014b].

Ray tracing studies have shown that the wave normal angle of chorus waves increases rapidly as the waves propagate from their generation region near the equator to higher latitudes, due to their refraction in the presence of an increasing geomagnetic field magnitude [*Breuillard et al.*, 2012; *Chen et al.*, 2013]. Such very oblique chorus waves have been observed on board various satellites [*Hayakawa et al.*, 1984; *Li et al.*, 2013a; *Agapitov et al.*, 2013]. During quiet or moderately disturbed geomagnetic conditions such that hot electrons do not damp oblique waves too strongly, pitch angle scattering by these waves can become dominant [*Mourenas et al.*, 2014; *Li et al.*, 2014b]. Moreover, their presence could lead to a growing total wave power from the equator up to latitudes $\lambda \sim 35°$ on the dayside [*Mourenas et al.*, 2014]. Inside the plasmasphere, VLF ($\sim$ 5–25 kHz) whistler mode waves generated by lightning discharges and naval transmitters often propagate at very oblique angles after having propagated past the equator along magnetic field lines [e.g., see *Abel and Thorne*, 1998; *Inan et al.*, 2010; *Agapitov et al.*, 2014, and references therein].

Accordingly, let us assume here a constant $\langle D_{\alpha\alpha}(\alpha_0)\rangle$, giving approximately $\tau_L \approx 1/(2\langle D_{\alpha\alpha}(\alpha_{LC})\rangle)$. Then, the one-dimensional pitch angle diffusion equation for the electron distribution reads as

$$\frac{\partial^2 g}{2\partial\alpha_0^2}\sin 2\alpha_0 + \frac{\partial g}{\partial\alpha_0}\cos 2\alpha_0 + g\sin 2\alpha_0 = 0 \tag{10}$$

The general analytical solution to equation (10) can be written as a combination of hypergeometric F and Meijer G functions [*Abramowitz and Stegun*, 1972] as

$$g(\alpha_0) = c_5 G_{2,2}^{2,0}\left(\cos^2\alpha_0 \,\middle|\, \frac{\left(1-\sqrt{3}\right)/2, \left(1+\sqrt{3}\right)/2}{0,\quad 0}\right) + c_6\, {}_2F_1\left(\left(1-\sqrt{3}\right)/2, \left(1+\sqrt{3}\right)/2, 1, \cos^2\alpha_0\right) \tag{11}$$

where the coefficients c_5 and c_6 can be determined the same way as before.

Figure 4 displays a comparison between electron distribution profiles obtained analytically, respectively, for parallel VLF waves and oblique VLF waves (i.e., for a constant $\langle D_{\alpha\alpha}(\alpha_0)\rangle$) interacting with 2 MeV electrons at $L \sim 2$ (similar results would be obtained for chorus waves at $L \sim 5$). An increase of the phase-space-density gradient downward from $\alpha_0 \sim 70°$ can be noticed when oblique waves are present as compared to the case of parallel waves alone, which may increase the growth rate of waves due to the distribution anisotropy [e.g., see *Kennel and Petschek*, 1966; *Johnstone et al.*, 1993; *Mourenas et al.*, 2014]. At $\alpha_0 > 70°$, conversely, the slope of g is very similar in both cases because very oblique waves are assumed to be mostly present away from the equatorial region. The induced change in the phase-space-density profile is too weak, however, to allow inferring the presence or not of very oblique waves from the sole analysis of measured profiles of the electron distribution.

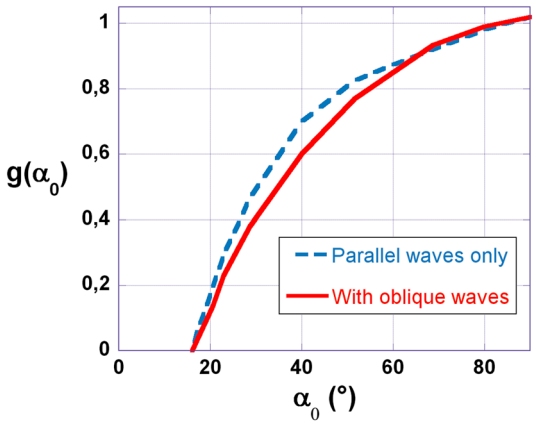

Figure 4. Profile of the (unnormalized) asymptotic (final) electron distribution in the case of 2 MeV electrons interacting with VLF waves at $L \sim 2$. The dashed blue line shows the approximate analytical solution given by equations (4) and (5) for parallel waves only, while the red curve shows the analytical solution (11) corresponding to a constant $\langle D_{\alpha\alpha}(\alpha_0)\rangle$ (with waves more oblique at higher latitudes and/or increasing wave power with latitude).

2.5. Analytical Electron Distributions When Taking Into Account Energization

Neglecting mixed diffusion (which can be important too) [see *Albert*, 2009] and assuming an initially cold distribution without high-energy electrons (for instance, just after dropouts) [e.g., see *Turner et al.*, 2013, and references therein], the energy broadening of the electron distribution $F(E,t)$ in the presence of quasi-linear energy diffusion by quasi-parallel whistler mode waves is given approximately by [*Horne et al.*, 2005; *Balikhin et al.*, 2012]

$$\frac{\partial F}{\partial t} = \frac{\partial}{\partial E}(A(E)\langle D_{EE}\rangle \frac{\partial (F/A(E))}{\partial E}) - \frac{F}{\tau_L} \quad (12)$$

where $A(E) \sim (E+0.511)\sqrt{E(E+1)}$ with E in MeV.

The solution is [*Balikhin et al.*, 2012; *Mourenas et al.*, 2014]

$$F(t) \propto E^{-4(1-\beta)} t^{-\beta} \exp\left(-\frac{E^2}{4\langle D_{EE}\rangle\, t} - \frac{t}{\tau_L}\right), \quad (13)$$

with $\beta \sim 5/4$ for $E < 0.5$ MeV and $\beta \sim 3/2$ for $E > 1$ MeV. Approximate analytical expressions for the bounce-averaged energy diffusion rate $\langle D_{EE}\rangle$ of electrons by quasi-parallel whistler mode waves have already been obtained [*Mourenas et al.*, 2012a, 2014]. Since the energization of the electron distribution by parallel waves mainly occurs at medium to high pitch angles [*Horne et al.*, 2005; *Mourenas et al.*, 2014], one can roughly take it into account by using the formula of $\langle D_{EE}\rangle$ given by equation (A6) in Appendix A, which generally remains approximately correct as long as $\alpha_0 > 15°$ [*Mourenas et al.*, 2012a].

The electron distribution F at high energy first increases quickly with time then reaches a maximum at a time t_{max} given by

$$t_{max} \approx \frac{\tau_L}{2}\left(-\beta + \sqrt{\beta^2 + \frac{E^2}{\langle D_{EE}\rangle\, \tau_L}}\right). \quad (14)$$

and later on decreases with the usual loss timescale τ_L.

However, a more complete diffusion equation must take into account *both* pitch angle and energy diffusion coefficients [*Glauert and Horne*, 2005; *Albert*, 2009], giving for the full electron distribution f:

$$\frac{\partial f}{\partial t} = \frac{\partial}{\partial E}(A(E)\langle D_{EE}\rangle \frac{\partial (f/A(E))}{\partial E}) + \frac{1}{T_b \sin 2\alpha_0}\frac{\partial}{\partial \alpha_0}(\langle D_{\alpha\alpha}\rangle T_b \sin 2\alpha_0 \frac{\partial f}{\partial \alpha_0}) \quad (15)$$

In order to obtain approximate but useful and insightful analytical solutions to the complex two-dimensional differential equation (15), some important simplifications must be made. Namely, we consider the case of an initially cold distribution (without high-energy electrons) scattered by quasi-parallel waves. In order to roughly evaluate the temporal variation of the phase space density f, we further assume in a first step that one can roughly separate energy and pitch angle variations and replace $f(E,t,\alpha_0)$ by $\sim F(E,t,\alpha_0 = 90°)g(\alpha_0)$ in equation (15), since the energization-related increase of f is mainly determined by the stronger rate $\langle D_{EE}\rangle$ at higher pitch angles [*Mourenas et al.*, 2012a, 2014]. Then, the slowest pitch angle scattering near the loss cone generally determines the loss rate for parallel chorus waves [*Mourenas et al.*, 2014; *Albert and Shprits*, 2009] and the energy diffusion term on the right-hand side of (15) should dominate during strong energization periods, yielding the approximate analytical solution (13) for $F(E,t)$.

Next, to evaluate the pitch angle shape of f, it is essential to take into account the slower energization at smaller α_0, i.e., the variation of $\langle D_{EE} \rangle \sim \sin \alpha_0$ in $F(t)$ (e.g., see equation (A6) in Appendix A) [*Mourenas et al.*, 2012a] and to replace now $f(E, t, \alpha_0)$ by $\sim F(E, t, \alpha_0) g(\alpha_0)$ in (15), with F given by (13). A close inspection of the various resulting terms shows that for $E^2/(4\langle D_{EE}(\alpha_0 \sim \pi/2)\rangle t) > 1$ during significant energization periods (i.e., for $t < t_{max}$ when $\langle D_{EE}(\pi/2)/E^2 \rangle \tau_L < 1$ and for $t < \beta t_{max}$ when $\langle D_{EE}(\pi/2)/E^2 \rangle \tau_L \geq 1$), the terms coming from $\partial F/\partial \alpha_0$ should prevail in the equation for $g(\alpha_0)$. Considering $\alpha_0 = 30° - 45°, t \sim t_{max}$, and nearly constant pitch angle diffusion, it leads roughly to

$$4t \left\langle \frac{D_{EE}(\pi/2)}{E^2} \right\rangle \sin \alpha_0 \tan \alpha_0 \frac{\partial^2 g}{\partial \alpha_0^2} + 2\frac{\partial g}{\partial \alpha_0} - \frac{g}{\tan \alpha_0} = 0$$

or $2(\partial g/\partial \alpha_0) \approx g/\tan \alpha_0$ and an approximate form $g \approx \sqrt{\sin \alpha_0}$ very weakly varying with α_0.

Actually, this shape of the g part of the full solution is very close to the steady state solution (4) for g obtained in a situation without energization. Nevertheless, its variation at very small α_0 is smoother, leading us to keep this last formulation. One important caveat of the present simplified analytical model is the assumption that fluxes at high energy are produced only through energy broadening of an initially cold distribution so that $f(t = 0, E) = 0$ at high E [e.g., *Balikhin et al.*, 2012]. In practice, however, the initial electron distribution $f(t = 0, E)$ is never null even at high energy. Thus, we must add the value of $f_0(t = 0, E)$ initially present (in simulations or observations) at high energy to the analytical distribution $f(t, E)$ given by equations (13) and (4). It leads finally to an approximate analytical solution to the full two-dimensional differential equation (15):

$$f(E, t, \alpha_0) \sim f_0(E, t = 0, \alpha_0) + F(E, t, \alpha_0 = \pi/2) \times \sqrt{\sin \alpha_0} \exp\left(\frac{E^2(\eta(\alpha_0) - 1)}{4\eta(\alpha_0)\langle D_{EE}(\pi/2)\rangle t}\right) \quad (16)$$

where F is given by equations (13), $\eta = \min(1, \sin \alpha_0/\sin \alpha_{0,m})$, and $\alpha_{0,m} = \min\left(\sin^{-1}\sqrt{0.9\Omega_{ce0}/(\gamma\omega_m)}, \pi/4\right)$. As a result, one finds that the global shape of the pitch angle distribution should be mainly determined by energization at early times $t \leq t_{max}$ due to the strong variation of the source F with $\alpha_0 < 40°$ in (13) via $\langle D_{EE}(\alpha_0)\rangle$. The above solution (16) is rather different from the late-time steady state solution g, due to the strong effect of energization included through F.

However, due to the presence of a denser core population injected already at 0.1–0.5 MeV initially (at $t = 0$), the above approximate formulation (16), based on the assumption of progressive energy broadening of a cold population, can only be used (i) at high-enough energies $E \geq E_{min} \geq 1$ MeV far away from the initial core population temperature, (ii) when strong energization occurs at $E > E_{min}$, and (iii) over a restricted time frame $\Delta t < \tau_{max}(E_{min})$ before energization vanishes at $E \leq E_{min}$ in the simplified model. The reason for the latter condition is that contrary to the simplified model's assumption, in real situations the energization does not stop, in general, at $t \geq \tau_{max}(E_{min})$ on the lower energy side ($E \leq E_{min}$) of the population, due to the remaining presence of a much denser peak of electrons at lower energies, coming from the initially injected hot population and which can still be further accelerated (e.g., see next section). As a result, the above simplified model of energy broadening can only be used for high-enough energy $E > \max(E_{min}, 1\ \text{MeV})$ with E_{min} given by condition (iii) with equations (13) and (14):

$$E_{min}[\text{MeV}] \sim \frac{t^{1/2}\ \langle B_w^2 \rangle^{1/2}\ \Omega_{ce0}^{3/4}\ \omega_m^{1/4}}{8[\text{pT} \cdot \text{s/rad}^{1/2}]\Omega_{pe0}^{3/2} \tan^{1/2} \Delta\theta}. \quad (17)$$

where the wave amplitude B_w is in pT, angular frequencies in rad/s, and $t = \Delta t$ in seconds is the elapsed time since the start of strong energization. Therefore, expression (16) is only (approximately) valid inside a restricted parameter domain (i.e., mainly at high-enough energy), and great care must be exerted when using it to describe storm time energization of electrons.

2.6. Validations of Analytical Distributions During Strong Energization Periods

Let us assume a situation of strong acceleration of relativistic (> 2 MeV) electrons by intense parallel chorus waves at $L \sim 5$, such that $\langle D_{EE}/E^2 \rangle \tau_L \geq 1$. Such a situation actually corresponds to two storms (of 9 October 2012 and 17 March 2013) recently simulated by *Thorne et al.* [2013] and *Li et al.* [2014a]. A comprehensive study of these two storms has shown that quasi-linear diffusion by measured intense parallel chorus waves

was primarily controlling highly energetic (> 100 keV) electron acceleration in the region where the peak in electron phase space density was observed in both cases [*Thorne et al.*, 2013; *Li et al.*, 2014a].

To validate the proposed analytical model of distribution, we have compared the evolution of f obtained from equation (16) with the results of numerical simulations from *Thorne et al.* [2013] and *Li et al.* [2014a] for these two storms. The latter authors have split the magnetic local time (MLT) and UT time into different sectors, corresponding to different values of (measured) wave intensity B_w^2, latitudinal range of wave presence, $\Omega_{pe0}/\Omega_{ce0}$ and ω_m/Ω_{ce0} ratios, and plasma density values. To simplify calculations of analytical distributions and to demonstrate the capabilities of the proposed method, we chose to use values averaged over MLT and UT. This average was, however, performed in such a way that the average energy diffusion rate $\langle D_{EE}\rangle/E^2$ given by equation (A6) be correct. To this aim, we first calculated the exact average values of the normalized energy diffusion rate $\langle D_n\rangle = \langle\langle B_w^2\rangle_{UT}\Omega_{ce0}^{3/2}\omega_m^{1/2}/\Omega_{pe0}^3\rangle_{MLT}$ from Table 1 in *Thorne et al.* [2013] at $L \sim 5$ and from Table 1 in *Li et al.* [2014a] at $L \sim 4.25$. Then, using simple averages over MLT sectors of the weakly varying parameters $\Omega_{pe0}/\Omega_{ce0}$ and ω_m/Ω_{ce0}, we adjusted the remaining parameters (plasma density N_e and B_w^2) to recover the exact average value of $\langle D_n\rangle$.

This gave us the following initial conditions for the storms of 9 October 2012 (17 March 2013): $\Omega_{pe0}/\Omega_{ce0} \sim 3(3.3)$, $\omega_m/\Omega_{ce0} \sim 0.23(0.22)$, $N_e \sim 4.4(12)$ cm^{-3}, and $\sqrt{\langle B_w^2\rangle} \sim 85(113)$ pT. Besides, the behavior of $f(t)$ should be better modeled in the vicinity of its maximum at $t \sim t_{max}(E)$ given by equation (14), where temporal variations are weaker. Thus, we have normalized f to its value in the Fokker-Planck simulations near the time $t_{max}(E)$ where f reaches its maximum, choosing a not-too-high energy $E = E_{norm} > E_{min}$, 1 MeV (far enough from the temperature of the initial distribution) for which strong energization occurs. The calculation time in $f(t)$ is the elapsed time since the beginning of the simulation, and we normalize $F(E,t,\alpha_0) = F(E,t,\alpha_0)f_{sim}(t_{max,sim}(E_{norm}),E_{norm})/F(t_{max},E_{norm})$ at $\alpha_0 = 90°$, where $f_{sim}(t_{max,sim}(E_{norm}),E_{norm})$ is taken from the simulations. Here we consider $E_{norm} = 2.3$ MeV, giving $t_{max,sim}(E_{norm}) \sim 12$ UT ($f \sim 9\cdot10^{-6}$) on 9 October 2012 and $t_{max,sim}(E_{norm}) \sim 24$ UT ($f \sim 2.5\cdot10^{-6}$) on 17 March 2013.

To estimate lifetimes τ_L, which vary with the parameter $\Omega_{pe0}/\Omega_{ce0}$ slightly differently than $1/\langle D\rangle$ [see *Mourenas et al.*, 2012b, Appendix A and equation (19)], we must only consider in Table 1 from *Thorne et al.* [2013] or *Li et al.* [2014a] the latitude range $\lambda > 25°$ where resonance with > 2 MeV electrons occurs. Keeping the other average parameters unchanged, it leads to MLT-averaged values for the storms of 9 October 2012 (17 March 2013) of $\sqrt{\langle B_w^2\rangle} \sim 48(57)$ pT. One can check that $\langle D_{EE}/E^2\rangle\tau_L \geq 1$ in both cases. Then, a limited error on the magnitude of lifetimes should not affect analytical estimates of f, because particle acceleration occurs much faster than losses.

Figure 5 shows that the analytical estimates of the distributions from equation (16) are in reasonable agreement with the full numerical simulations from $E \sim 2$ MeV to $E \sim 6$–7 MeV for both geomagnetic storms, in spite of the different parameters. While $f(E,t)$ varies over 6 orders of magnitude, the global mean relative error between analytical estimates and simulation results at $\alpha_0 > 45°$ remains only a factor of ~ 2 and a factor ~ 2.5 over $\alpha_0 = 20°$–$90°$. Here one gets $t_{max} \sim 0.75(2.5)$ days for 2.3(4.5) MeV for the October 2012 storm and $t_{max} \sim 0.8(4.8)$ days for 2.3(5.6) MeV for the storm in March 2013. The end time of the simulations is therefore close to t_{max}(2.3 MeV) where a saturation of energization should occur at $E \sim 2.3$ MeV. However, electron energization is still building up at higher energies. An increasing discrepancy between simulations and estimates can be noticed as α_0 decreases below 20°. It is probably related to the limiting condition $\partial f/\partial\alpha_0 = 0$ for $\alpha_0 = 0$ used in the simulations *Li et al.* [2014a], whereas the part (13) of the analytical solution tends toward zero at $\alpha_0 = 0$. Some differences could also stem from mixed (pitch angle and energy) diffusion which is neglected in estimates and from the consequences of a nonnull $f(E,t=0)$ in the simulations.

The evolution of the full electron energy spectrum is also displayed in Figure 5 (right) as a function of time for the March 2013 storm, at two different L shells. At $L = 3.5$, we made use again of wave and plasma parameters obtained as a function of time and MLT from POES satellites and the Van Allen Probes [*Li et al.*, 2014a] to derive the average parameters needed for the model. We found $\Omega_{pe0}/\Omega_{ce0} \sim 2.6$, $\omega_m/\Omega_{ce0} \sim 0.22$, $N_e \sim 32$ cm^{-3}, and $\sqrt{\langle B_w^2\rangle} \sim 97$ pT. We are still in a situation such that $\langle D_{EE}/E^2\rangle\tau_L \geq 1$. It can be clearly seen that due to the dense core population (the first gray slope in Figure 5, right) already present at 0.3–0.6 MeV initially (at $t = 0$ in simulations, corresponding to 12 UT on 17 March 2013), the simplified model of energy broadening of an initially cold population can be used only at high-enough energies $E > E_{min} \sim 1.5$–2 MeV.

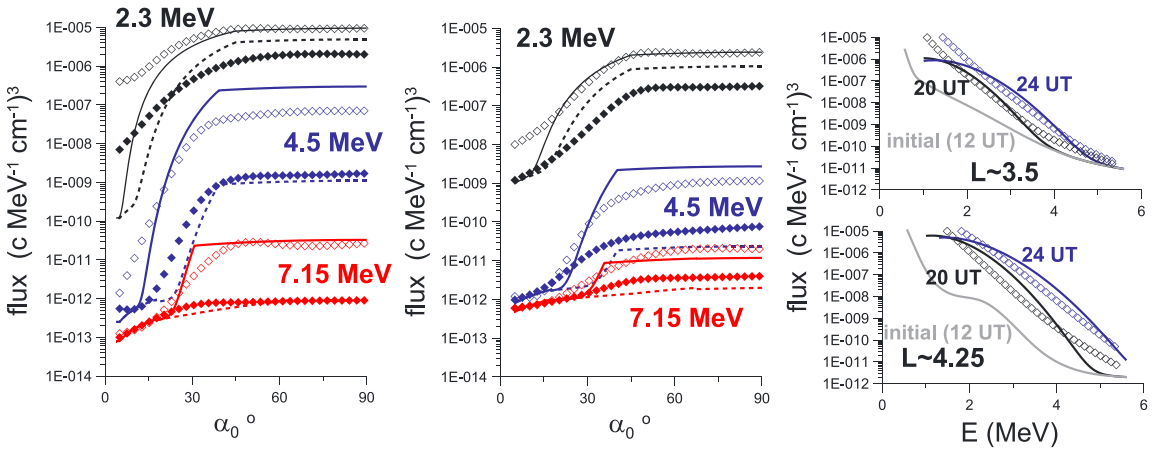

Figure 5. Profiles of the electron distribution $f(E, t, \alpha_0)$ in the case of high-energy electrons interacting with lower band chorus waves (left) at $L \sim 5$ during the storm of 9 October 2012 [*Thorne et al.*, 2013] and (middle) at $L \sim 4.25$ during the storm of 17 March 2013 [*Li et al.*, 2014a]. Analytical solutions from equation (16), normalized at $\alpha_0 = \pi/2$ to the simulation's value at the end time for $E = 2.3$ MeV, are plotted for end times $t = 12$ UT (universal time) on 9 October 2012 and $t = 24$ UT on 17 March 2013 (large solid lines). Analytical solutions are also displayed for $t = 8$ UT on 9 October 2012 and $t = 20$ UT on 17 March 2013 (dashed lines). Simulations and analytical calculations start at $t = 20$ UT on 8 October 2012 and at $t = 12$ UT on 17 March 2013. Open (filled) symbols show values of the corresponding numerical simulations from *Thorne et al.* [2013] for $t = 12(8)$ UT on 9 October 2012 and from *Li et al.* [2014a] for $t = 24(20)$ UT on 17 March 2013. (right) The evolution of the electron energy spectra (at $\alpha_0 = 90°$) as a function of time during the storm of 17 March 2013 at $L \sim 4.25$ and 3.5: simulation results (black and blue symbols), analytical solutions (black and blue lines), and initial energy spectrum (fitted to Van Allen Probes measurements, gray line).

Nevertheless, the temporal evolution of this high-energy shoulder of the electron distribution, far away from the bulk of the initial distribution, appears to be roughly reproduced by the model (16) from 2 MeV to 6 MeV (see Figure 5, right). As usual, higher-energy fluxes start to increase later than lower energy fluxes. But the electron energy spectrum over $E \sim 2$–5 MeV quickly takes a shape which does not depend on the much smaller initial flux levels in this range. During this March 2013 storm, energization also turns out to be significantly stronger at $L = 4.25$ than at $L = 3.5$, coinciding with the highest chorus wave intensities [*Li et al.*, 2014a].

2.7. Using Analytical Distributions During Strong Energization Periods to Estimate Average Chorus Intensity

To demonstrate the potential usefulness of the above approximate analytical solutions, we shall try here to infer the value of the average parallel chorus wave intensity from an analysis of the measured energized electron distribution (from its important variations with time and energy) performed with the help of equation (16). Assuming a strong storm in the region $3.5 \leq L \leq 5.5$ accompanied by chorus-induced energization such that $\langle D_{EE}/E^2 \rangle \tau_L \geq 1$ and $\langle D_{EE}/E^2 \rangle t \ll 1$ as above, one gets the following relationship for two energies E_1 and $E_2 > E_1$ and $\alpha_0 > 45°$ at a given time t after the start of the strong energization period:

$$\frac{E_2^2}{\langle D_{EE}(E_2) \rangle} - \frac{E_1^2}{\langle D_{EE}(E_1) \rangle} \sim -4t \ln\left(\frac{f(E_2)E_1^2}{f(E_1)E_2^2}\right) \tag{18}$$

leading finally to

$$\frac{\langle B_w^2 \rangle \Omega_{ce0}^{3/2} \omega_m^{1/2}}{100[\mathrm{pT}^2 \cdot \mathrm{s}^2/\mathrm{rad}] \Omega_{pe0}^3 \tan \Delta\theta} \sim \frac{-1}{2t} \times \left(\frac{E_2^{3/2}(1+2E_2)}{\sqrt{1+E_2}} - \frac{E_1^{3/2}(1+2E_1)}{\sqrt{1+E_1}} \right) / \ln\left(\frac{f(E_2)E_1^2}{f(E_1)E_2^2}\right) \tag{19}$$

with E_1 and E_2 in MeV, the average amplitude B_w in pT, angular frequencies in rad/s, and t in seconds is the elapsed time since the beginning of strong energization (for instance, since the start of the storm recovery phase). Equation (19) shows that if the ratio $f(E_2)/f(E_1)$ has been measured by a satellite and if in addition one can use some reasonably good estimates (or even better, in situ measurements) of the average values of ω_m/Ω_{ce0}, Ω_{ce0}, $\Delta\theta$, and Ω_{pe0}, it is possible in principle to derive an estimate of the averaged (over latitude and MLT) chorus wave intensity at latitudes $\lambda < 20°$ during the considered storm. Note that one needs only a *ratio* of fluxes at different energies at a same time, which should get us rid of at least part of the

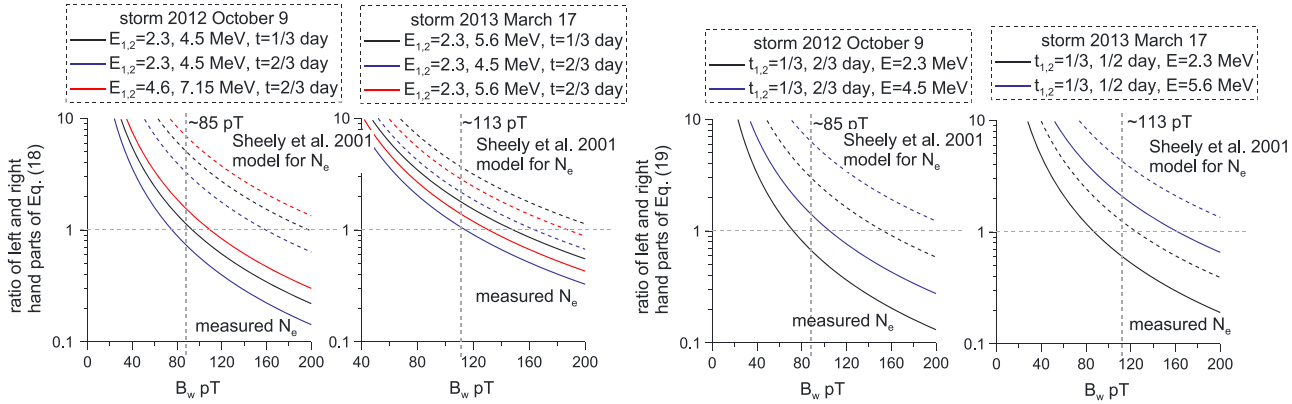

Figure 6. Estimates of the RMS chorus wave amplitude $\sqrt{\langle B_w^2 \rangle}$ during two geomagnetic storms (9 October 2012 and 17 March 2013) on the basis of ratios of electron fluxes measured by the Van Allen Probes [*Thorne et al.*, 2013; *Li et al.*, 2014a] at different times and for different energies, making use of equations (19) and (20). The ratio of the left- and right-hand parts of equation (19) or (20) is plotted so that the estimated amplitude is given by the intersection of the curves with the horizontal dashed line at 1. We use either the plasma trough density model of *Sheeley et al.* [2001] (dashed lines) or the more precise average density obtained from the Van Allen Probes (solid lines). The RMS chorus wave amplitudes directly measured by the Van Allen Probes or inferred from POES measurements [*Thorne et al.*, 2013; *Li et al.*, 2014a] are indicated by vertical dashed lines.

uncertainties related to flux measurements. Moreover, the resulting estimate of $\langle B_w^2 \rangle$ varies only like the logarithm of this flux ratio, mitigating the uncertainties related to the use of approximate analytical formulas for f. $\langle B_w^2 \rangle$ varies with other parameters like $\sim N_e^{3/2}/(t\Omega_{ce0}^{3/2})$. The magnitude of the geomagnetic field can deviate from its dipolar value due to field line stretching in the midnight sector during strongly disturbed periods. Nevertheless, the MLT-averaged deviation generally remains smaller than 30% even during strong storms [*Thorne et al.*, 2013; *Li et al.*, 2014a] in the considered region $3.5 \leq L \leq 5.5$. Apart from the flux ratio, the most important parameter is therefore the average plasma density N_e, which can depart very significantly from its average statistical value [*Sicard-Piet et al.*, 2014].

Alternatively, one can consider a given energy E and use the measured ratio $f(t_2, E)/f(t_1, E)$ at two different times during the same period. It gives

$$\frac{\langle B_w^2 \rangle \Omega_{ce0}^{3/2} \omega_m^{1/2}}{100[\mathrm{pT}^2 \cdot \mathrm{s}^2/\mathrm{rad}]\Omega_{pe0}^3 \tan\Delta\theta} \sim \frac{(t_2 - t_1)}{2t_1 t_2} \times \left(\frac{E^{3/2}(1+2E)}{\sqrt{1+E}} \right) / \ln\left(\frac{f(t_2)t_2^{3/2}}{f(t_1)t_1^{3/2}} \right) \quad (20)$$

where this estimate of $\langle B_w^2 \rangle$ varies like the logarithm of the flux ratio and with other parameters like $\sim N_e^{3/2}/(t_1 t_2 \Omega_{ce0}^{3/2})$. Thus, it depends much more than the previous estimate on a precise determination of the starting time of strong energization.

To assess the reliability of the proposed method, we have applied it to the same two geomagnetic storms (of 9 October 2012 and 17 March 2013) as before. Now, however, we are using the levels of electron phase space density *measured* by the Van Allen Probes during each storm at different energies and at different times [*Thorne et al.*, 2013; *Li et al.*, 2014a] to infer various estimates of $\langle B_w^2 \rangle$. To this aim, we simply use average statistical values $\omega_m/\Omega_{ce0} \simeq 0.25$, $\Delta\theta = 30°$, Ω_{ce0} from a dipolar geomagnetic field, and either the average plasma trough density model $N_e \simeq 100(3/L)^4$ cm^{-3} from *Sheeley et al.* [2001] or the 2–3 times smaller average measured value of the plasma density given above.

One can see in Figure 6 that the chorus waves RMS amplitudes deduced from analytical estimates (19) and (20) are in very good agreement with average measured amplitudes during both storms when using the measured plasma density value. In such a case, one obtains a mean error percentage smaller than ~ 20% between RMS amplitudes calculated with (19) and (20) and RMS amplitudes directly measured by the Van Allen Probes or inferred from Polar-orbiting Operational Environmental Satellites (POES) measurements [*Thorne et al.*, 2013; *Li et al.*, 2013b, 2014a; *Ni et al.*, 2014]. Moreover, the maximum deviation from the measured average amplitude remains smaller than a factor ~ 1.5. However, when using a statistical average of the density [*Sheeley et al.*, 2001], wave amplitudes can be overestimated by a mean factor ~ 2. This is due

to the lower than average plasma density measured during both storms. Using statistically averaged values for the other parameters does not affect significantly the estimated wave amplitudes.

In principle, the analytical solutions could therefore be used to infer RMS chorus wave amplitudes from energetic electron flux measurements during storms, provided that the plasma density can be determined accurately enough. This method could be employed, for instance, during periods when directly measured or POES-inferred wave amplitudes are not available or too uncertain or to supplement the existing wave databases. However, even if the above results are promising, they should mainly be considered as means of double checking the validity of the analytical solutions (i.e., the validity of the underlying assumptions and approximations) in two clean case studies where chorus-induced electron energization was known to prevail. Deriving wave amplitudes from real observations in a lot of different cases will probably prove to be a more difficult task. In reality, electron acceleration by chorus waves can mingle with various other processes, like acceleration by magnetosonic waves, radial diffusion [e.g., see *Li et al.*, 2014a], or enhanced pitch angle scattering by electromagnetic ion cyclotron (EMIC) waves, making it harder to evaluate the exact role played by chorus waves.

Nevertheless, occurrence rates of intense EMIC waves are very low, near 2.6% over $4 < L < 7$ during active periods, with an average $\Omega_{pe0}/\Omega_{ce0}$ ratio generally larger than 10 and time-averaged intensities smaller than 0.3 nT [*Meredith et al.*, 2014]. Moreover, EMIC waves have been shown to scatter only moderate pitch angle particles at $\alpha_0 < 45°$–$60°$ [*Usanova et al.*, 2014], not affecting the bulk of the energized population at higher pitch angles that we are interested in here. Intense fast magnetosonic waves may also efficiently accelerate electrons of a few MeV in the outer radiation belt [*Horne et al.*, 2007]. However, the corresponding energy diffusion rate generally peaks at energies such that $\gamma \approx 6\Omega_{ce0}/\Omega_{pe0}$ and decreases at higher energy like $1/\gamma^3 \sim 1/E^3$ [*Mourenas et al.*, 2013], while for chorus waves the energy diffusion rate decreases continuously but less quickly than $1/E^2$. Furthermore, energy diffusion by magnetosonic waves should be mainly important for large $\Omega_{pe0}/\Omega_{ce0} > 7$ and then mainly limited to some narrow pitch angle domain [*Mourenas et al.*, 2013]. Thus, an energization dominated by fast magnetosonic waves should lead to some peak of energization at a moderate-energy value and a progressively smaller influence than chorus waves as E increases. In principle, identifying the presence of such a maximum in measured electron fluxes might be feasible and could help to remove the corresponding energy range from consideration when estimating chorus wave intensity by the above proposed method. Moreover, very high RMS amplitudes of magnetosonic waves, larger than about 4 times the chorus waves RMS amplitudes, would be needed to have a strong effect [e.g., see *Mourenas et al.*, 2013, Figure 11]. During disturbed periods of enhanced chorus activity, magnetosonic waves should consequently not strongly affect, in general, the mean value of the inferred chorus wave amplitudes.

The pitch angle profile of the analytical distributions can also be compared with the measured profiles at different energies and times. Analytical fits to $f(t, E)$ at $\alpha_0 > 45°$ already provide estimates of the RMS wave amplitude which are only weakly dependent on ω_m/Ω_{ce0}. However, the steep decrease of $f(\alpha_0)$ toward low α_0 is mainly determined by $\sin\alpha_{0,m} \approx \sqrt{\Omega_{ce0}/\omega_m\gamma}$. In this case, one can obtain best analytical fits to the measured $f(E, t, \alpha_0)$ by minimizing the global standard deviation over $\alpha_0 = 20°$–$90°$ at different energies and times, looking now for an optimum couple of values $(\omega_m, \langle B_w^2\rangle)$. For the storm of October 2012, we found accordingly $\omega_m/\Omega_{ce0} \sim 0.20$ and $\sqrt{\langle B_w^2\rangle} \sim 92$ pT, close to the average measured values. Provided that strong EMIC waves are not simultaneously present, it might be possible to estimate this way both the average frequency and amplitude of the chorus waves from electron flux measurements. It would be especially useful for storms during which no direct wave measurements (and no other alternative techniques) are available, but it could also complement other existing techniques. Conversely, in cases where wave intensity, wave frequency, and geomagnetic field values are already known, the same formulas (19) and (20) could be used to infer the unknown average plasma density. The proposed method could therefore help to build event-specific as well as global wave and plasma models required to drive large-scale radiation belt codes during disturbed periods. Before that, however, the general applicability of this method needs to be tested statistically in a variety of real (sometimes complex) situations, which is left for a further dedicated study.

3. Discussion and Conclusions

As briefly discussed above, one potentially useful application of the preceding analytical solutions could be to provide a new method to estimate the MLT-averaged and latitude-averaged wave characteristics from only few measurements of the electron distribution in different energy ranges. This opportunity can be important because a substantial part of satellite measurements of wave parameters corresponds to the near-equatorial region, while wave characteristics strongly vary along field lines [e.g., see *Mourenas et al.*, 2014]. In contrast, electron velocity distributions measured in the vicinity of the equator have been modified by resonant interactions with waves over a large range of latitudes, and as a result, the structure of these distributions *remembers* the properties of waves in the unmeasurable regions.

At low $L < 3.5$ during quiet times, when quasi-parallel hiss whistler mode waves are interacting with not-too-high energy electrons, the obtained pitch angle distributions are peaked at 90° (see Figure 3). The measured location of a sudden drop of $g(\alpha_0)$ near 70°–80° would then give directly $\alpha_{0,i}$ and therefore the upper frequency cutoff of the hiss spectrum. The slopes of the different parts of g depend directly through (9) on the wave parameters ω_m/Ω_{ce0} and $\Delta\theta$. Thus, using precise measurements of g at various energies could allow to determine these parameters. Finally, using these determined parameters and comparing the measured global lifetimes with their analytical counterparts could help to provide an estimate of the bounce-averaged and azimuthal drift-averaged wave power. The latter would be a valuable complement to localized wave measurements on board satellites.

During very disturbed geomagnetic conditions when mainly parallel chorus waves are controlling the strong energization of relativistic electrons in the outer belt [*Chen et al.*, 2013; *Thorne et al.*, 2013; *Li et al.*, 2014a; *Mourenas et al.*, 2014], the variations of $f(E, t, \alpha_0 > 45°)$ can be compared with the corresponding analytical solutions to gain some indirect knowledge of the MLT-averaged wave power at latitudes $\lambda < 20°$, provided that the intensity of fast magnetosonic waves is not too high and radial diffusion is not too strong near the L location of the maximum of energization (see previous section).

During weaker (and slower) energization periods in the outer belt, such that $\langle D_{EE}(\pi/2)/E^2\rangle \tau_L \ll 1$, comparisons of analytical solutions with measured electron fluxes could allow to estimate the value of $t_{max} \sim \tau_L/\sqrt{4\tau_L\langle D_{EE}(\pi/2)/E^2\rangle}$ at various electron energies E. It would give the ratio of $\langle D_{EE}(\pi/2)\rangle$ (proportional to B_w^2 near the equator) to $\langle D_{\alpha\alpha}(\alpha_{LC})\rangle$ (proportional to B_w^2 at increasing latitudes for increasing E; see Appendix A), therefore providing the variation of the MLT-averaged wave power with latitude. In this case, however, one needs to assume that EMIC waves and radial diffusion have a smaller effect on the flux decay than chorus waves. During more quiet times outside of the plasmasphere, the existence of an exponential decay of measured fluxes could also be used to deduce the averaged (over latitude and MLT) chorus wave intensity by means of comparisons of observed lifetimes of electrons with analytical estimates of lifetimes at various energies (see Appendix A) [*Mourenas et al.*, 2012b; *Artemyev et al.*, 2013b; *Mourenas et al.*, 2014; *Li et al.*, 2014b]. However, the observed decay timescales can also be influenced by electron injections at low energy and by EMIC waves or outward radial diffusion at high energy, especially at high $L \sim 6$ [*Boynton et al.*, 2014], requiring a very cautious approach. Indeed, discrepancies between the simplified analytical solutions and numerical solutions or observations are expected to increase as the situation becomes more complex (as already seen from Figures 2–5). Therefore, more numerous validations of the methods outlined above by comparisons with measured average wave amplitudes are definitely required but left for future work.

In summary, we have derived here general analytical expressions for the energy and pitch angle distribution of trapped electrons in the radiation belts. The analytical distributions are approximate solutions to the exact two-dimensional Fokker-Planck equation governing the distribution function when quasi-linear diffusion of high-energy (> 1 MeV) electrons in pitch angle and energy by limited amplitude (< 300 pT) whistler mode waves is the dominant process. The analytical solutions have been successfully compared with full numerical results. Used in combination with measured electron distributions provided by the Van Allen Probes, they allowed us to recover the measured average amplitude of chorus waves during two storms. The satisfactory agreement with both observations and full simulations opens the door to future investigations of observed trapped particle distributions performed with the help of the presented analytical formulations. Such comparisons could help to improve our global understanding of the active processes and provide useful estimates of the wave's characteristic features.

Appendix A: Analytical Expressions for Lifetimes and Diffusion Rates

An approximate analytical formulation of the electron lifetime at relatively low energy (for $1.1 < p\epsilon_m < p\epsilon_{UC} < 10$) due to Landau resonance pitch angle diffusion by whistler mode waves has already been derived by *Mourenas and Ripoll* [2012] and *Artemyev et al.* [2013b] for a quasi-parallel wave normal angle distribution $G(\theta) = \exp(-\tan^2\theta/\tan^2\Delta\theta)$ where $\Delta\theta < 45°$ is the characteristic width of the distribution. It reads as

$$\tau_{LL} \approx \frac{B_0^2|1-\omega_m/\Omega_{ce0}|^{-3/2}}{3\gamma B_w^2\Omega_{ce0}}\left(\frac{p\Omega_{pe0}}{\Omega_{ce0}}\right)^4\frac{\tan\Delta\theta}{\sin^3\alpha_{M0}} \times \frac{\frac{\pi}{2}-\alpha_{0,i}-\frac{2}{3}\sin 2\alpha_{0,i}-\frac{1}{12}\sin 4\alpha_{0,i}}{G(\theta_{M0})+\min(C^3/11, C^{-1})} \tag{A1}$$

Here B_0 is the equatorial geomagnetic field magnitude, $C = p\varepsilon_m\tan\Delta\theta$, ω_m is the mean frequency of the wave (at peak power B_w^2), $\alpha_{0,i} = 1/(p\epsilon_{UC})$ is the highest equatorial pitch angle where cyclotron resonance exists, $\theta_{M0} \approx \tan^{-1}(1.84/p\varepsilon_m)$ is the wave normal angle at peak equatorial Landau resonance, and $\cos\alpha_{M0} \approx |1-\omega_m/\Omega_{ce0}|^{1/2}\gamma\omega_m/(\Omega_{ce0}p\varepsilon_m)$ gives the location of the Landau resonance scattering peak. The waves which dominate in the Landau part of the lifetime and which must therefore be considered here are such that they have the highest value of wave power B_w^2 multiplied by $G(\theta_{M0}) + \min(C^3/11, C^{-1})$. It corresponds to hiss or VLF waves (the latter at very low L) in the plasmasphere and lower band chorus in the outer belt. Nevertheless, ω_{UC} as well as ϵ_{UC} and $\alpha_{0,i}$ are always determined by the upper frequency cutoff of the highest-frequency quasi-parallel waves.

The minimum in pitch angle scattering occurring at $\alpha_0 \sim \alpha_{0,i}$ is given by the Landau resonance diffusion rate at this location. It can be written approximately as [*Mourenas and Ripoll*, 2012; *Artemyev et al.*, 2013b]

$$\left\langle D_{\alpha\alpha}(\alpha_{0,i})\right\rangle \approx \frac{\gamma B_w^2\Omega_{ce0}^5\sin^3\alpha_{M0}}{2p^4B_0^2\Omega_{pe0}^5\tan\Delta\theta}\frac{\left|1-\omega_m/\Omega_{ce0}\right|^{3/2}}{\cos^3\alpha_{0,i}\sin\alpha_{0,i}} \times\left(G(\theta_{M0})+\min\left(C^3/11, C^{-1}\right)\right) \tag{A2}$$

The diffusion coefficient for first-order cyclotron resonance is obtained after integration over bounce motion [*Lyons et al.*, 1972], considering the smallest-frequency and highest-intensity parallel waves (hiss or lower band chorus). Near the loss cone edge, one finds [*Mourenas and Ripoll*, 2012; *Artemyev et al.*, 2013b]

$$\langle D_{\alpha\alpha}(\alpha_{LC})\rangle \approx \frac{\pi B_w^2\Omega_{ce0}\,\omega_m}{4\gamma B_0^2\Delta\omega(p\varepsilon_m)^{13/9}\,T_b(\alpha_{LC})\cos^2\alpha_{LC}}\times \times\frac{\Delta\lambda_{R,N}(1+3\sin^2\lambda_R)^{7/12}(1-\varpi)}{|\gamma\varpi-2\gamma\varpi^2+1|\,|1-\gamma\varpi|^{4/9}} \tag{A3}$$

where $\varpi = \omega_m/(\Omega_{ce0}(p\varepsilon_m)^{2/3})$, $T_b(\alpha_{LC}) \approx 1$, and the latitude of resonance λ_R for $\omega \approx \omega_m$ can be written as

$$\lambda_R^2 \sim \frac{3}{2}-\frac{3}{2}\sqrt{1-\frac{16}{9}\left(1-\left(\frac{|1-\gamma\varpi|}{p\varepsilon_m\sqrt{\cos\Delta\theta}}\right)^{1/9}\right)} \tag{A4}$$

The latitudinal range of resonance corresponding to $\Delta\omega$ is $\Delta\lambda_R \sim 2(\sqrt{\lambda_R^2+2\Delta\omega/(27\omega_m)/(p\varepsilon_m)^{1/9}}-\lambda_R)$ when the waves exist up to the highest latitudes [*Mourenas et al.*, 2012b]. But when the waves are confined to $\lambda < \lambda^+$, the actual latitudinal range of resonance becomes $\Delta\lambda_{R,N} \sim \max(\min(\lambda^+, \lambda_R+\Delta\lambda_R/2)-\lambda_R+\Delta\lambda_R/2, 0)$ [*Artemyev et al.*, 2013b].

The loss timescale $\tau_{L<}$ corresponding to the sole region $\alpha_{LC} < \alpha_0 < \alpha_{0,i}$ is given by the integral of $1/(4\langle D_{\alpha\alpha}\rangle\tan\alpha_0)$ over the same domain for cyclotron-resonance wave-particle interaction [*Mourenas and Ripoll*, 2012]:

$$\tau_{L<} \sim \frac{2\ln(\sin\alpha_{0,i}/\sin\alpha_{LC})+\cos^2\alpha_{0,i}-\cos^2\alpha_{LC}}{8\,\langle D_{\alpha\alpha}(\alpha_{LC})\rangle} \tag{A5}$$

Finally, an approximate analytical expression of the bounce-averaged quasi-linear energy diffusion coefficient of electrons interacting with fixed-amplitude parallel waves can be derived [*Mourenas et al.*, 2012a, 2014]. Refined estimates for $p\epsilon_m > 6$ yield a variation with α_0 weaker than $\sin\alpha_0$ at $\alpha_0 > 45°$ as in simulations and show that $\langle D_{EE}\rangle/E^2$ decreases approximately by a factor $\sin\alpha_0$ more quickly below $\alpha_{0,m} \sim \min(\sin^{-1}\sqrt{0.9\Omega_{ce0}/(\gamma\omega_m)}, \pi/4)$ than at $\alpha_0 > 45°$ (see equations (10), (12), and (17) in *Mourenas et al.* [2012a] and equation (10) in *Mourenas et al.* [2012b]), in agreement with numerical simulations [*Mourenas et al.*, 2012a, Figure 1]. Taking the latter dependencies into account , we get

$$\frac{\langle D_{EE}\rangle}{E^2}\left[\frac{1}{s}\right] \approx \frac{B_w^2\,\Omega_{ce0}^{3/2}\omega_m^{1/2}}{100[pT^2\cdot s^2/rad]}\,\frac{(\gamma+1)^{1/2}\eta(\alpha_0)\Omega_{pe0}^{-3}}{\tan\Delta\theta\gamma(\gamma-1)^{3/2}} \tag{A6}$$

where $\eta = \min(1, \sin\alpha_0/\sin\alpha_{0,m})$. The above formula has been checked to remain roughly correct down to $\alpha_0 \sim 15°$. Note that in equations (A1), (A2), and (A6), B_w^2 denotes the average wave power from mainly low latitudes (between $\lambda = 0°$ and $\lambda \sim 20°$), while it represents in equation (A3) the average power between $\lambda_R - \Delta\lambda_{R,N}/2$ and $\lambda_R + \Delta\lambda_{R,N}/2$ (i.e., at higher λ for higher E).

Acknowledgments

All the new data used in this paper are obtained from analytical solutions of equations (3), (10), and (15). Corresponding parameters and boundary conditions are listed in the text. Work of A.V.A. was partially supported by the grant MK-1781.2014.2. The work at UCLA was supported by the EMFISIS subaward 1001057397:01, ECT subaward 13-041, and NASA grants NNX11AD75G, NNX11AR64G, NNX12AD12G, and NNX13AI61G.

Michael Liemohn thanks Yue Chen and another reviewer for their assistance in evaluating this paper.

References

Abel, B., and R. M. Thorne (1998), Electron scattering loss in Earth's inner magnetosphere: 2. Sensitivity to model parameters, *J. Geophys. Res.*, *103*, 2397–2407, doi:10.1029/97JA02920.

Abramowitz, M., and I. A. Stegun (1972), *Handbook of Mathematical Functions With Formulas, Graphs, and Mathematical Tables*, Dover, New York.

Agapitov, O., A. Artemyev, V. Krasnoselskikh, Y. V. Khotyaintsev, D. Mourenas, H. Breuillard, M. Balikhin, and G. Rolland (2013), Statistics of whistler mode waves in the outer radiation belt: Cluster STAFF-SA measurements, *J. Geophys. Res. Space Physics*, *118*, 3407–3420, doi:10.1002/jgra.50312.

Agapitov, O., A. Artemyev, D. Mourenas, Y. Kasahara, and V. Krasnoselskikh (2014), Inner belt and slot region electron lifetimes and energization rates based on AKEBONO statistics of whistler waves, *J. Geophys. Res. Space Physics*, *119*, 2876–2893, doi:10.1002/2014JA019886.

Albert, J. M. (1994), Quasi-linear pitch-angle diffusion coefficients: Retaining higher harmonics, *J. Geophys. Res.*, *99*, 23,741–23,745, doi:10.1029/94JA02345.

Albert, J. M. (2009), The coupling of quasi-linear pitch angle and energy diffusion, *J. Atmos. Sol. Terr. Phys.*, *71*, 1664–1668, doi:10.1016/j.jastp.2008.11.014.

Albert, J. M., and Y. Y. Shprits (2009), Estimates of lifetimes against pitch angle diffusion, *J. Atmos. Sol. Terr. Phys.*, *71*, 1647–1652, doi:10.1016/j.jastp.2008.07.004.

Artemyev, A., O. Agapitov, D. Mourenas, V. Krasnoselskikh, and L. Zelenyi (2013a), Storm-induced energization of radiation belt electrons: Effect of wave obliquity, *Geophys. Res. Lett.*, *40*, 4138-4143, doi:10.1002/grl.50837.

Artemyev, A., D. Mourenas, O. Agapitov, and V. Krasnoselskikh (2013b), Parametric validations of analytical lifetime estimates for radiation belt electron diffusion by whistler waves, *Ann. Geophys.*, *31*, 599–624, doi:10.5194/angeo-31-599-2013.

Baker, D. N., J. B. Blake, L. B. Callis, J. R. Cummings, D. Hovestadt, S. Kanekal, B. Klecker, R. A. Mewaldt, and R. D. Zwickl (1994), Relativistic electron acceleration and decay time scales in the inner and outer radiation belts: SAMPEX, *Geophys. Res. Lett.*, *21*, 409–412, doi:10.1029/93GL03532.

Baker, D. N., et al. (2014), Gradual diffusion and punctuated phase space density enhancements of highly relativistic electrons: Van Allen Probes observations, *Geophys. Res. Lett.*, *41*, 1351–1358, doi:10.1002/2013GL058942.

Balikhin, M., M. Gedalin, G. D. Reeves, R. J. Boynton, and S. A. Billings (2012), Time scaling of the electron flux increase at GEO: The local energy diffusion model vs observations, *J. Geophys. Res.*, *117*, A10208, doi:10.1029/2012JA018114.

Boynton, R. J., M. A. Balikhin, and D. Mourenas (2014), Statistical analysis of electron lifetimes at GEO: Comparisons with chorus-driven losses, *J. Geophys. Res. Space Physics*, *119*, 6356–6366, doi:10.1002/2014JA019920.

Brautigam, D. H., and J. M. Albert (2000), Radial diffusion analysis of outer radiation belt electrons during the October 9, 1990, magnetic storm, *J. Geophys. Res.*, *105*, 291–309, doi:10.1029/1999JA900344.

Breuillard, H., Y. Zaliznyak, V. Krasnoselskikh, O. Agapitov, A. Artemyev, and G. Rolland (2012), Chorus wave-normal statistics in the Earth's radiation belts from ray tracing technique, *Ann. Geophys.*, *30*, 1223–1233, doi:10.5194/angeo-30-1223-2012.

Bunch, N. L., M. Spasojevic, and Y. Y. Shprits (2013), The spectral extent of chorus in the off-equatorial magnetosphere, *J. Geophys. Res. Space Physics*, *118*, 1700–1705, doi:10.1029/2012JA018182.

Chen, L., R. M. Thorne, W. Li, and J. Bortnik (2013), Modeling the wave normal distribution of chorus waves, *J. Geophys. Res. Space Physics*, *118*, 1074–1088, doi:10.1029/2012JA018343.

Glauert, S. A., and R. B. Horne (2005), Calculation of pitch angle and energy diffusion coefficients with the PADIE code, *J. Geophys. Res.*, *110*, A04206, doi:10.1029/2004JA010851.

Hayakawa, M., Y. Yamanaka, M. Parrot, and F. Lefeuvre (1984), The wave normals of magnetospheric chorus emissions observed on board GEOS 2, *J. Geophys. Res.*, *89*, 2811–2821, doi:10.1029/JA089iA05p02811.

Horne, R. B., R. M. Thorne, S. A. Glauert, J. M. Albert, N. P. Meredith, and R. R. Anderson (2005), Timescale for radiation belt electron acceleration by whistler mode chorus waves, *J. Geophys. Res.*, *110*, A03225, doi:10.1029/2004JA010811.

Horne, R. B., R. M. Thorne, S. A. Glauert, N. P. Meredith, D. Pokhotelov, and O. Santolík (2007), Electron acceleration in the Van Allen radiation belts by fast magnetosonic waves, *Geophys. Res. Lett.*, *34*, L17107, doi:10.1029/2007GL030267.

Horne, R. B., S. A. Glauert, N. P. Meredith, D. Boscher, V. Maget, D. Heynderickx, and D. Pitchford (2013), Space weather impacts on satellites and forecasting the Earth's electron radiation belts with SPACECAST, *Space Weather*, *11*, 169–186, doi:10.1002/swe.20023.

Inan, U. S., S. A. Cummer, and R. A. Marshall (2010), A survey of ELF and VLF research on lightning-ionosphere interactions and causative discharges, *J. Geophys. Res.*, *115*, A00E36, doi:10.1029/2009JA014775.

Johnstone, A. D., D. M. Walton, R. Liu, and D. A. Hardy (1993), Pitch-angle diffusion of low energy electrons by whistler mode waves, *J. Geophys. Res.*, *98*, 5959–5967, doi:10.1029/92JA02376.

Kennel, C. F., and H. E. Petschek (1966), Limit on stably trapped particle fluxes, *J. Geophys. Res.*, *71*, 1–28.
Li, W., J. Bortnik, R. M. Thorne, C. M. Cully, L. Chen, V. Angelopoulos, Y. Nishimura, J. B. Tao, J. W. Bonnell, and O. LeContel (2013a), Characteristics of the Poynting flux and wave normal vectors of whistler-mode waves observed on THEMIS, *J. Geophys. Res. Space Physics*, *118*, 1461–1471, doi:10.1002/jgra.50176.
Li, W., B. Ni, R. M. Thorne, J. Bortnik, J. C. Green, C. A. Kletzing, W. S. Kurth, and G. B. Hospodarsky (2013b), Constructing the global distribution of chorus wave intensity using measurements of electrons by the POES satellites and waves by the Van Allen Probes, *Geophys. Res. Lett.*, *40*, 4526–4532, doi:10.1002/grl.50920.
Li, W., et al. (2014a), Radiation belt electron acceleration by chorus waves during the 17 March 2013 storm, *J. Geophys. Res. Space Physics*, *119*, 4681–4693, doi:10.1002/2014JA019945.
Li, W., et al. (2014b), Evidence of stronger pitch angle scattering loss caused by oblique whistler-mode waves as compared with quasi-parallel waves, *Geophys. Res. Lett.*, *41*, 6063–6070, doi:10.1002/2014GL061260.
Lyons, L. R. (1974), Pitch angle and energy diffusion coefficients from resonant interactions with ion-cyclotron and whistler waves, *J. Plasma Phys.*, *12*, 417–432, doi:10.1017/S002237780002537X.
Lyons, L. R., R. M. Thorne, and C. F. Kennel (1972), Pitch-angle diffusion of radiation belt electrons within the plasmasphere, *J. Geophys. Res.*, *77*, 3455–3474, doi:10.1029/JA077i019p03455.
Meredith, N. P., R. B. Horne, S. A. Glauert, D. N. Baker, S. G. Kanekal, and J. M. Albert (2009), Relativistic electron loss timescales in the slot region, *J. Geophys. Res.*, *114*, A03222, doi:10.1029/2008JA013889.
Meredith, N. P., et al. (2012), Global model of lower band and upper band chorus from multiple satellite observations, *J. Geophys. Res.*, *117*, A10225, doi:10.1029/2012JA017978.
Meredith, N. P., et al. (2014), Global morphology and spectral properties of EMIC waves derived from CRRES observations, *J. Geophys. Res. Space Physics*, *119*, 5328–5342, doi:10.1002/2014JA020064.
Mourenas, D., and J. F. Ripoll (2012), Analytical estimates of quasi-linear diffusion coefficients and electron lifetimes in the inner radiation belt, *J. Geophys. Res.*, *117*, A01204, doi:10.1029/2011JA016985.
Mourenas, D., A. Artemyev, O. Agapitov, and V. Krasnoselskikh (2012a), Acceleration of radiation belts electrons by oblique chorus waves, *J. Geophys. Res.*, *117*, A10212, doi:10.1029/2012JA018041.
Mourenas, D., A. V. Artemyev, J.-F. Ripoll, O. V. Agapitov, and V. V. Krasnoselskikh (2012b), Timescales for electron quasi-linear diffusion by parallel and oblique lower-band Chorus waves, *J. Geophys. Res.*, *117*, A06234, doi:10.1029/2012JA017717.
Mourenas, D., A. Artemyev, O. Agapitov, and V. Krasnoselskikh (2013), Analytical estimates of electron quasi-linear diffusion by fast magnetosonic waves, *J. Geophys. Res. Space Physics*, *118*, 3096–3112, doi:10.1002/jgra.50349.
Mourenas, D., A. Artemyev, O. Agapitov, and V. Krasnoselskikh (2014), Consequences of geomagnetic activity on energization and loss of radiation belt electrons by oblique chorus waves, *J. Geophys. Res. Space Physics*, *119*, 2775–2796, doi:10.1002/2013JA019674.
Ni, B., W. Li, R. M. Thorne, J. Bortnik, J. C. Green, C. A. Kletzing, W. S. Kurth, G. B. Hospodarsky, and M. de Soria-Santacruz Pich (2014), A novel technique to construct the global distribution of whistler mode chorus wave intensity using low-altitude POES electron data, *J. Geophys. Res. Space Physics*, *119*, 5685–5699, doi:10.1002/2014JA019935.
O'Brien, T. F., et al. (2014), An empirically observed pitch-angle diffusion eigenmode in the Earth's electron belt near L*=5, *Geophys. Res. Lett.*, *41*, 251–258, doi:10.1002/2013GL058713.
Schulz, M., and L. J. Lanzerotti (1974), *Particle Diffusion in the Radiation Belts*, Springer, New York.
Sheeley, B. W., M. B. Moldwin, H. K. Rassoul, and R. R. Anderson (2001), An empirical plasmasphere and trough density model: CRRES observations, *J. Geophys. Res.*, *106*, 25,631–25,642, doi:10.1029/2000JA000286.
Shprits, Y. Y., et al. (2006), Acceleration mechanism responsible for the formation of the new radiation belt during the 2003 Halloween solar storm, *Geophys. Res. Lett.*, *33*, L05104, doi:10.1029/2005GL024256.
Shprits, Y. Y., D. A. Subbotin, N. P. Meredith, and S. R. Elkington (2008), Review of modeling of losses and sources of relativistic electrons in the outer radiation belt II: Local acceleration and loss, *J. Atmos. Sol. Terr. Phys.*, *70*, 1694–1713, doi:10.1016/j.jastp.2008.06.014.
Sicard-Piet, A., D. Boscher, R. B. Horne, N. P. Meredith, and V. Maget (2014), Effect of plasma density on diffusion rates due to wave particle interactions with chorus and plasmaspheric hiss: Extreme event analysis, *Ann. Geophys.*, *32*, 1059–1071, doi:10.5194/angeo-32-1059-2014.
Su, Z., F. Xiao, H. Zheng, and S. Wang (2011), CRRES observation and STEERB simulation of the 9 October 1990 electron radiation belt dropout event, *Geophys. Res. Lett.*, *38*, L06106, doi:10.1029/2011GL046873.
Summers, D., R. M. Thorne, and F. Xiao (1998), Relativistic theory of wave-particle resonant diffusion with application to electron acceleration in the magnetosphere, *J. Geophys. Res.*, *103*, 20,487–20,500, doi:10.1029/98JA01740.
Tao, X., J. Bortnik, J. M. Albert, and R. M. Thorne (2012), Comparison of bounce-averaged quasi-linear diffusion coefficients for parallel propagating whistler mode waves with test particle simulations, *J. Geophys. Res.*, *117*, A10205, doi:10.1029/2012JA017931.
Thorne, R. M. (2010), Radiation belt dynamics: The importance of wave-particle interactions, *Geophys. Res. Lett.*, *372*, L22107, doi:10.1029/2010GL044990.
Thorne, R. M., et al. (2013), Rapid local acceleration of relativistic radiation belt electrons by magnetospheric chorus, *Nature*, *504*, 411–414, doi:10.1038/nature12889.
Trakhtengerts, V. Y. (1966), Stationary states of the Earth's outer radiation zone, *Geomag. Aeron.*, *6*, 827–836.
Turner, D. L., V. Angelopoulos, W. Li, M. D. Hartinger, M. Usanova, I. R. Mann, J. Bortnik, and Y. Shprits (2013), On the storm-time evolution of relativistic electron phase space density in Earth's outer radiation belt, *J. Geophys. Res. Space Physics*, *118*, 21960–2212, doi:10.1002/jgra.50151.
Usanova, M. E., et al. (2014), Effect of EMIC waves on relativistic and ultrarelativistic electron populations: Ground-based and Van Allen Probes observations, *Geophys. Res. Lett.*, *41*, 1375–1381, doi:10.1002/2013GL059024.